Oceanological and Hydrobiological Studies

International Journal of Oceanography and Hydrobiology

Volume 47, Issue 4, December 2018
pages (415-428)

ISSN 1730-413X
eISSN 1897-3191

Wind characteristics and wind energy assessment in the Barents Sea based on ERA-Interim reanalysis

by

Chenglin Duan, Zhifeng Wang*, Sheng Dong, Zhenkun Liao

DOI: **10.1515/ohs-2018-0039**
Category: **Original research paper**
Received: **February 2, 2018**
Accepted: **April 26, 2018**

College of Engineering, Ocean University of China, Qingdao 266100, China

Abstract

The basic analysis of long-term wind characteristics and wind energy resources in the Barents Sea was carried out from 1996 to 2015 based on the ERA-Interim reanalysis dataset from ECMWF. In recent years, it has been possible to exploit the wind power resources in the Barents Sea at the hub height due to the sea ice cover retreat in the northeast direction. Based on the NSDIC monthly sea ice concentration data, the entire Barents Sea has been partitioned into the ice-free zone and the ice zone. Spatial and temporal distributions of the mean monthly and annual wind speed and wind power density are presented in both zones. Seven points were selected at different locations in the ice-free zone so as to obtain and study the wind roses, the interannual wind power variation and the annual average net electric energy output. For extreme wind speed parameters, the Pearson type III distribution provides better fitness of annual speed extrema and the Gumbel distribution performs well with higher speeds at longer return periods.

Key words: sea ice zoning, offshore wind, wind energy, spatio-temporal variation, extreme wind parameters, Barents Sea

* Corresponding author: *wzf1984@ouc.edu.cn*

DE GRUYTER

The *Oceanological and Hydrobiological Studies* is online at www.oandhs.pl

Introduction

In recent years, the energy-related environmental issues have attracted more attention than before. We are confronted with rising levels of greenhouse gas emissions in the atmosphere as well as with a shortage of conventional fossil fuels. Meanwhile, new and clean renewable energy resources have been available, such as solar, wind, hydrogen, bioenergy, waves, tides, currents and geothermal energy (Gasparatos et al. 2017).

Offshore wind energy has become the major sustainable source of new electricity due to its less negative impact on environment. Therefore, basic knowledge of sea surface wind climate is essential for planning and installing wind power generators. In this respect, assessments of offshore wind conditions and energy resources have so far been conducted in various regions of the world, such as America (Chadee & Clarke 2014), Latin America (Simionato et al. 2005), Africa (Alimi et al. 2005), Asia (e.g. Zheng et al. 2013; Wang et al. 2016), Europe (e.g. Karamanis et al. 2011; Ban et al. 2013; Onea 2015) and at a global scale (Liu et al. 2008; Capps & Zender 2009; 2010; Zheng & Pan 2014; Eurek et al. 2017). In the meantime, various offshore wind turbines have been designed and methodologies have been proposed to evaluate and optimize the electricity-generation capacity (Eriksson et al. 2008; Yang et al. 2014).

The Barents Sea has a unique geographical advantage and less sea ice cover compared with other seas at the same latitudes, such as the Chukotka Sea and the Laptev Sea. In particular, the wind power resources in the Barents Sea can be exploited with the accelerating decrease of the sea ice cover. The analysis proposed by Shapiro et al. (2003) shows that the mean ice edge location has significantly retreated to the northeast. Since 2005, the sea ice area has declined rapidly in the Barents Sea, reaching a minimum value of 400 000 compared to the previous value of 670 000 km^2 (Herbaut et al. 2015). Therefore, it has become possible that wind resources can be exploited in the ice-free area of the Barents Sea. Changes in the atmospheric thermal stability caused by the reduction of the sea-ice cover in the region may well play an important role in changing the wind energy potential at the hub height. Based on the European Centre for Medium-Range Weather Forecasts (ECMWF) ERA-40 datasets for the period from 1957 to 2002, Reistad et al. (2011) used the dynamic atmospheric downscaling approach to get a high-resolution wind field in the Barents Sea. To our knowledge, however, other current literature on the wind field in the Barents Sea focused mainly on its dynamic and thermodynamic interaction with sea ice rather than long-term wind characteristics and wind power estimates (Ingvaldsen et al. 2004; Pavlova et al. 2014; Lien et al. 2017). Consequently, information on wind behavior is not sufficient to assess wind energy resources for engineering purposes.

There are no successive wind velocity observations in the open ocean, particularly in the Arctic and subarctic regions, because of uncertain errors resulting from *in situ* conditions, reading approaches and interpretation methods. Reanalysis data represent a complete integration and assimilation of both observed and modeled wind speeds. Thus, reanalysis data have been widely selected in many recent papers to enable a similar preliminary analysis in different areas (Simionato et al. 2005; Ban et al. 2013; Zheng et al. 2013; Chadee & Clarke 2014; Zheng & Pan 2014; Onea et al. 2015).

Wind energy resources at high latitudes have been gradually given more attention in recent years (Perković et al. 2013), but the relevant detailed assessment still remains blank. The main objective of this paper is to analyze the datasets from ECMWF ERA-Interim in order to characterize the wind climate, the available annual and seasonal average wind power density in the Barents Sea. The paper consists of 4 sections. The study area, data entry and methodology for assessing the wind behavior and power density are described in the Materials and methods. The sea ice zoning, distributions of wind fields, power density and available electricity power output are shown in the Results. The comparison with other regions and extreme wind speed parameters are presented in the Discussion. Finally, a summary and conclusions are given in the Conclusions.

Materials and methods

Description of ECMWF ERA-Interim datasets

The ECMWF is one of the most known centers for research on climate variability and has integrated the scientific and technical resources of Europe's meteorological services. Its ERA-Interim reanalysis program can provide global wind field datasets, including Arctic and subarctic regions. The ocean surface winds in ERA-Interim datasets have assimilated many conventional observational data throughout the reanalysis period, e.g. from ships, drifting buoys and offshore stations. Furthermore, additional scatterometer ocean surface wind data have also been used in ERA-Interim, including recalibrated data from ERS-1 and ERS-2, and data from QuikSCAT. Based on the rigorous procedure of data check and selection,

the observing system serves as an indispensable constraint to the atmospheric reanalysis (Dee et al. 2011). The quality of ERA-Interim reanalysis has been validated and verified in many researches (e.g. Dee & Uppala 2009; Dee et al. 2011; Hodges et al. 2011; Szczypta et al. 2011).

Study area and data description

Following the previous research on the Barents Sea (Lien et al. 2017), the domain covering 65°N to 85°N and 0°E to 65°E has been selected and analyzed in this study (Fig. 1).The Barents Sea is covered with sea ice in the northern and southeastern zones in winter, thus ice distributions should be taken into consideration.

The wind fields at 10 m were obtained from the ECMWF ERA-Interim reanalysis dataset for the period from 1996 to 2015. The dataset consists of daily wind velocity, including meridional and zonal components, measured four times a day (0 h, 6 h, 12 h and 18 h) and a spatial resolution of 0.25 × 0.25°. The monthly sea ice concentrations (SIC) were obtained from the National Snow and Ice Data Center (NSIDC) for the same period. The SIC were provided in the polar stereographic projection with a grid cell size of 25 × 25 km.

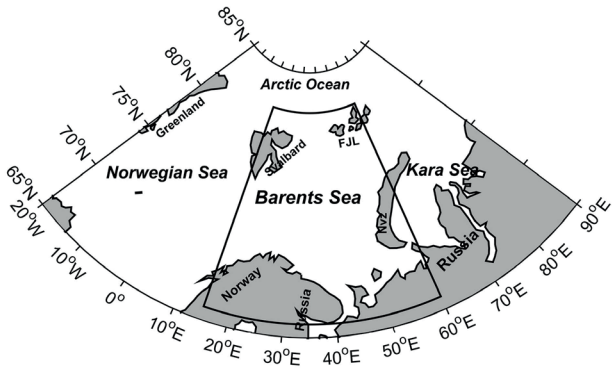

Figure 1

Geographical location of the Barents Sea and the sea area within the inner sector is the selected domain for the statistical study

Methods of determining the ice-free area

The coastal fast ice and drift ice can significantly jeopardize the operation safety of wind turbines. It is therefore important to isolate the ice-free zone from the whole domain. In particular, once the SIC exceeds 30%, sailing vessels and other offshore operations may have difficulties in maneuvering (Shapiro et al. 2003; Divine & Dick 2006). Therefore, the whole domain can be divided into the ice-free zone and the ice zone, using the mean monthly SIC isopleth of 30% as a boundary. The ice partitions can be described as:

$$\begin{aligned} &0 \le SIC < 30\%, && \text{Ice-free Zone;} \\ &SIC = 30\%, && \text{Ice Edege;} \\ &30\% < SIC \le 100\%, && \text{Ice Zone.} \end{aligned} \tag{1}$$

Methods of assessing the wind climate and energy

The wind speed at 10 m is calculated using the 6-hourly data:

$$V_{10} = \sqrt{u^2 + v^2} \tag{2}$$

where V_{10}, u, and v represent the total, meridional and zonal 10 m wind velocity, respectively.

In order to better understand wind speed and power density at the hub height (100 m), the power-law wind-profile equation was used (Panofsky & Dutton 1984):

$$\frac{V_{\text{zub}}}{V_{10}} = \left(\frac{Z_{\text{zub}}}{Z_{10}} \right)^P \tag{3}$$

where V_{zub} is the wind speed at the hub height Z_{zub}, and V_{10} and Z_{10} are already known wind speed and height, respectively. In this work, the power-law exponent P = 0.11 is adopted according to the previous study presented by Hsu et al. (1994).

The wind energy density is defined as the power per unit area perpendicular to the direction from which the wind blows. Thus, the wind power density, which relies on the wind speed and air density, can be expressed as:

$$E = \frac{1}{2} \rho V^3 \tag{4}$$

where E is the selected basic unit for computing the power stored in the wind and ρ is the air density. Clearly, it is easy to conclude that a small fluctuation in wind speed can cause a large difference in wind power density.

In addition, the factor of temperature was taken into account to calculate the air density. The temperature varies depending on the month and altitude above sea Z. Therefore, the corresponding air density can be calculated using the following equation (Fyrippis et al. 2010):

$$\rho = \rho_0 \frac{T_0}{T}\left(1-\frac{\Gamma Z}{T_0}\right)^{\frac{g}{\Gamma R}} \quad (5)$$

where g is the gravitational acceleration, T is the absolute temperature each month, T_0 = 288 K, R = 287 J deg^{-1} kg^{-1} is the ideal gas constant, ρ_0 = 1.225 kg m^{-3} is the standard sea level air density and r = 6.5 K^{-km} is the vertical temperature gradient, respectively.

In order to depict the spatial distribution of wind speed and power density, two equations (6–7) were used to describe the annual, seasonal and monthly mean speed and power density.

$$\bar{V} = \frac{1}{N}\sum_{i=1}^{N} V_i \quad (6)$$

$$\bar{E} = \frac{1}{N}\sum_{i=1}^{N} E_i \quad (7)$$

where N represents the total number of wind speed records.

Furthermore, the annual average extractable net electric energy output P can be approximately estimated as the product of all possible wind speeds multiplied by the power output $Pe(V_i)$ of the wind turbine curve given by a manufacturer. The equation provided by Karamanis et al. (2011) can be used:

$$P = \left(1-C_p\right)\frac{H_t}{N}\sum_{i=1}^{N} Pe(V_i) \quad (8)$$

where H_t represents the total number of hours per year and C_p = 10% is the ratio coefficient of required energy for internal controls and routine maintenance of turbines.

In addition, the design wind speeds with longer return periods are important for ocean engineering applications. We used four popular extreme value distribution functions – generalized extreme value (GEV), Gumbel, Weibull and Pearson type III (P-III) distribution – to estimate the extreme wind speeds. The Kolmogorov-Smirnov (K-S) test and the root mean square error (RMSE) method were used to determine which function is relatively better to fit the series of annual wind speed extrema. Formulas of the extreme value distribution functions are shown in Table 1.

Results

Distribution of the sea ice and ice zone partition

Based on the NSIDC sea ice concentrations, the monthly sea ice extent from January to December was calculated, with the minimum observed in September and the maximum in April. The results are consisted with the analysis presented by Kwok (2009). Consequently, the ice edge advances and retreats seasonally. In this paper, the ice-free zone actually refers to the ice-free zone throughout the year. Therefore, the SIC isoline of 30% in April and September can be regarded as a boundary between the ice-free zone, the seasonal ice zone and the multi-annual ice zone. The April ice-free zone can preserve the ice-free conditions throughout the year, which can hardly pose a serious threat to offshore wind farms. The distributions of ice, the ice zone partitions and the relevant ice edge positions are shown in Figure 2. High concentrations of sea ice are observed in winter in the northern and southeastern domains, while permanent open waters are observed

Table 1

Four extreme value distribution functions

Distribution type	Probability density distribution function $f(x)$	Parameters
GEV	$\frac{1}{\alpha}\left[1-\beta\left(\frac{v-\mu}{\alpha}\right)\right]^{1/\beta-1}\exp\left\{-\left[1-\beta\left(\frac{v-\mu}{\alpha}\right)\right]^{1/\beta}\right\}$	μ-location parameter α-scale parameter β-shape parameter
Gumbel	$\frac{1}{\alpha}\exp\left[-\left(\frac{v-\mu}{\alpha}\right)-\exp\left(-\frac{v-\mu}{\alpha}\right)\right]$	μ-location parameter α-scale parameter
Weibull	$\frac{\alpha}{\beta}(v-\mu)^{\alpha-1}\exp\left[-\frac{(v-\mu)^{\alpha}}{\beta}\right] \quad x \geq \mu$	μ-location parameter β-shape parameter α-scale parameter
P-III	$\frac{\beta^{\alpha}}{\Gamma(\alpha)}(v-\mu)^{\alpha-1}e^{-\beta(x-\mu)} \quad v^3\mu,\alpha>0$	μ-location parameter β-shape parameter α-scale parameter

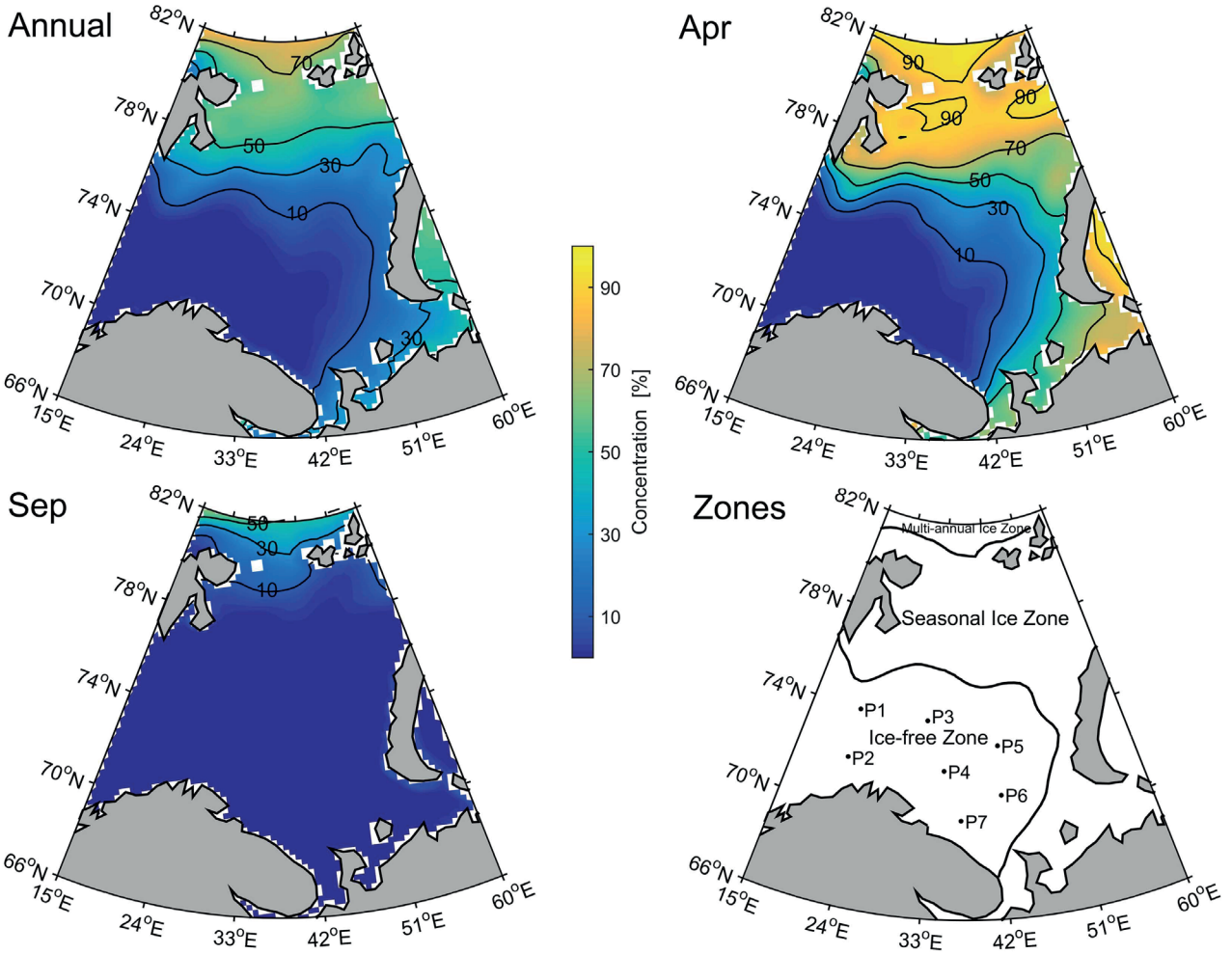

Figure 2

Annual average, mean monthly maximum (April), minimum (September) distributions of the sea ice concentration and the ice zone partitions. In the ice-free zone, the points labeled from P1 to P1 are selected for further wind climate and energy analysis.

throughout the year in the southeastern domain. In the open water zones (i.e. the ice-free zone), there are hardly any serious threats induced by drift or floating ice.

Sea surface meteorological study

Annual wind speed at 10 m analysis

By analyzing the 20-year wind datasets, the annual average spatial distribution of climatological wind speeds was calculated based on the average 6 h resolution data across the Barents Sea.

As shown in Figure 3, three conspicuous features are easy to observe. First of all, wind speeds between 6 and 8.5 m s^{-1} occur in most parts of the Barents Sea. The largest wind speed occurs in the southwest, which is even more than 8 m s^{-1}. Secondly, the wind speeds decrease from southwest to northeast in the domain. To be more specific, the wind speed isoline of 7.4 m s^{-1} approximately coincides with the boundary of the ice zone. Thirdly, the wind speeds in the coastal areas are relatively low and decline sharply toward the mainland. In particular, the offshore wind speeds are much higher compared to the inland wind speeds, which are less than 3.6 m s^{-1} in most areas.

Mean seasonal wind speed at 10 m analysis

In general, wind behavior is closely related to weather conditions. In other words, wind conditions may change from year to year, month to month and

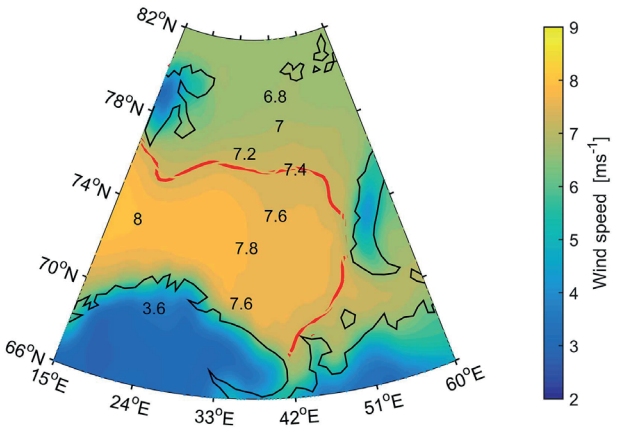

Figure 3

Spatial distributions of annual average wind speed at 10 m

day to day. Therefore, monthly analysis is important for a detailed understanding of temporal wind variations in the domain. Based on the average data of the same month in each year from 1996 to 2015, the mean monthly wind speeds for each month were calculated.

The strongest wind speeds occur in January, ranging from 8.5 to 10 m s^{-1} in the ice-free zone. On the other hand, the lowest wind speeds of less than 6.5 m s^{-1} occur in July (monthly wind figures are not shown herein). Therefore, based on the monthly results, a noticeable seasonal variation of wind speeds is recorded. Seasonal partitions presented by the World Meteorological Society was used in this study: winter (December–January–February), spring (March–April–May), summer (June–July–August) and autumn (September–October–November). Figure 4 shows spatial distributions of mean seasonal wind speeds from winter to autumn. The largest wind speed exceeding 9 m s^{-1} occurs in winter, while the lowest in summer. In winter, the offshore wind speeds are mostly 8.5–10 m s^{-1} in the ice-free zone and 7.5–8.5 m s^{-1} in the ice zone; in spring – 7.5–8.5 m s^{-1} in the ice-free zone and 6–7.5 m s^{-1} in the ice zone; in summer – approximately 5.5–6.5 m s^{-1} in the ice-free zone and 5–5.5 m s^{-1} in the ice zone; in autumn – approximately 7.5–8.5 m s^{-1} in the ice-free zone and 7–8 m s^{-1} in the ice zone.

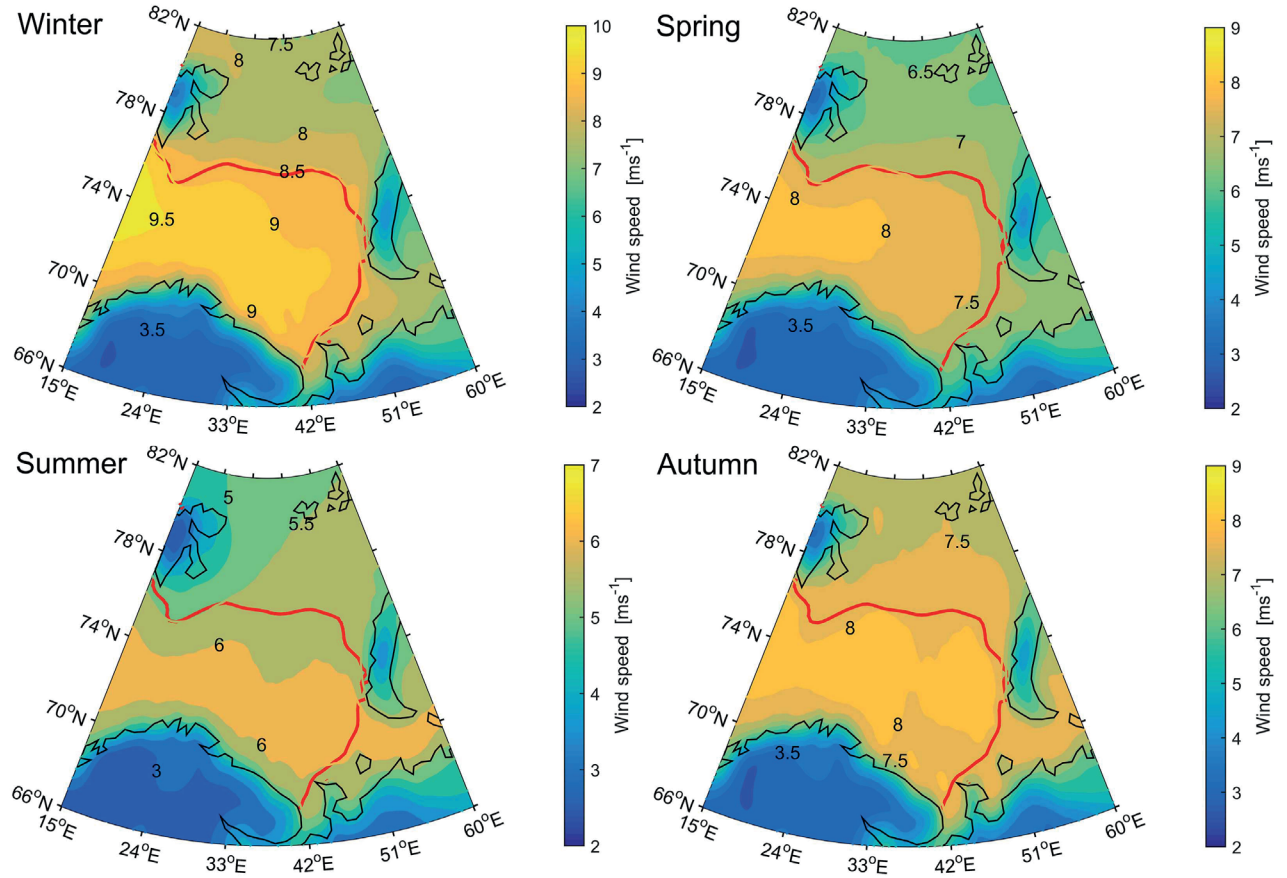

Figure 4

Spatial distributions of mean seasonal wind speed at 10 m from winter to autumn

Wind roses analysis

Wind directions are also highly dependent on weather conditions. Hence, the wind directions change yearly, seasonally, monthly and even daily. Therefore, in order to better understand wind behavior, it is important to study wind direction and proportional speed distributions. In this regard, seven points were selected in such a way as to cover all open sea water zones in their entirety. Figure 2 shows the geographical locations of the points labeled from P1 to P7.

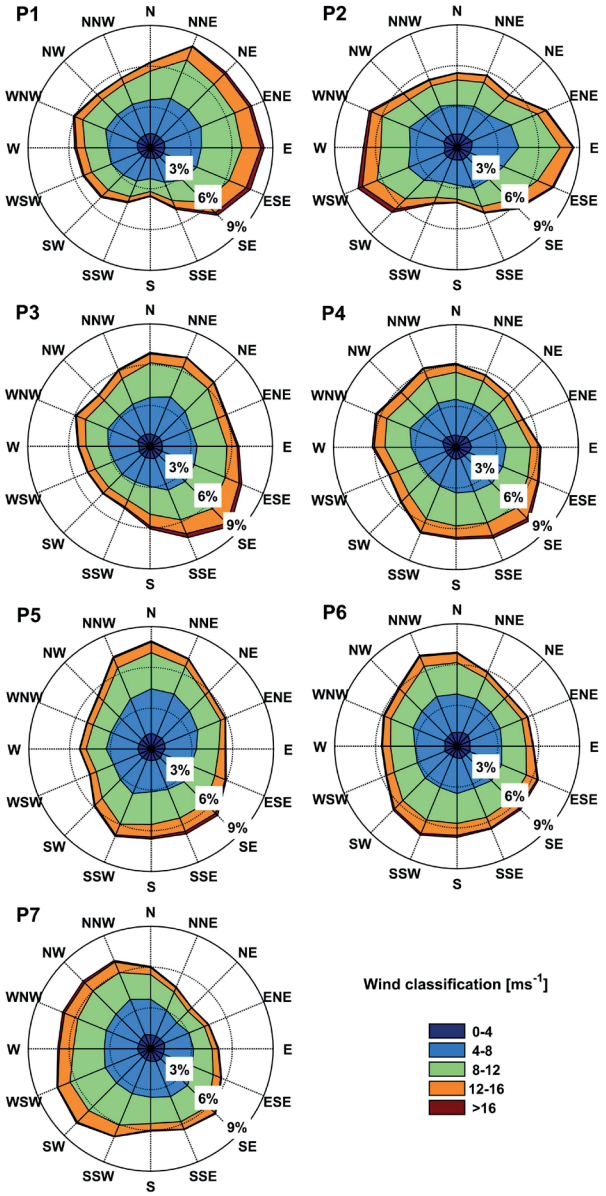

Figure 5

Wind roses from P1 to P7 in the Barents Sea. The color scale represents wind speed classification

Figure 5 illustrates the wind roses at the seven points based on the 20-year datasets. The directions from NNE to ESE play an important role in P1, while those from SW to WNW and from ENE to ESE are common in P2. In P3 and P4, SE wind is moderately dominant. In P5 and P6, directions from NNW to NNE and from SSW to SE are relatively common. In P7, directions from SW to NNW are more prevalent. The largest direction frequency is less than 10%. In addition, the wind speed was classified into five levels from 0 to > 16 m s^{-1} with the interval of 4 m s^{-1} (see the legend in Fig. 5). The high-frequency wind speeds are in the intervals of 4–8 m s^{-1} and 8–12 m s^{-1}.

Extractable and renewable wind power potential

Annual wind speed and power density at 100 m analysis

In order to assess the offshore wind energy production, it is very important to analyze in detail the wind conditions and power density at the hub height. Therefore, annual average spatial patterns of wind speeds and power density at 100 m were calculated according to equations (3–7). Such contour patterns are presented in Figure 6.

As shown in Figure 6, similar characteristics to wind conditions at 10 m were found. At 100 m height, wind speeds between 8.5 and 10.5 m s^{-1} with power density between 600 and 1200 W m^{-2} occur in most parts of the entire domain. The strongest wind speed and the largest wind energy occur in the southwest – even more than 10 m s^{-1} and 1000 W m^{-2}, respectively. In particular, the wind speed isoline of 9.5 m s^{-1} and the energy isoline of 900 W m^{-2} is in good agreement with the ice zone boundary. Therefore, the ice-free region is characterized by high speed and rich power density. In addition, the wind speed and power density decline rapidly toward the land in the nearshore zones.

Seasonal wind speed and power density at 100 m analysis

As mentioned above, the wind climate as well as the contained wind power potential are largely dependent on weather conditions. Thus, monthly and seasonal analysis is necessary to determine temporal variations. In the monthly analysis, January has the largest wind speeds and power density, while July is the calmest month. Figures 7 and 8 show spatial distributions of mean seasonal wind speed and power density at 100 m in each month.

It appears from Figure 7 that the average wind speed in the ice-free zone may exceed 11 m s^{-1} in winter and the speed is still above 7.5 m s^{-1} in summer. Regarding the power density presented in Figure 8,

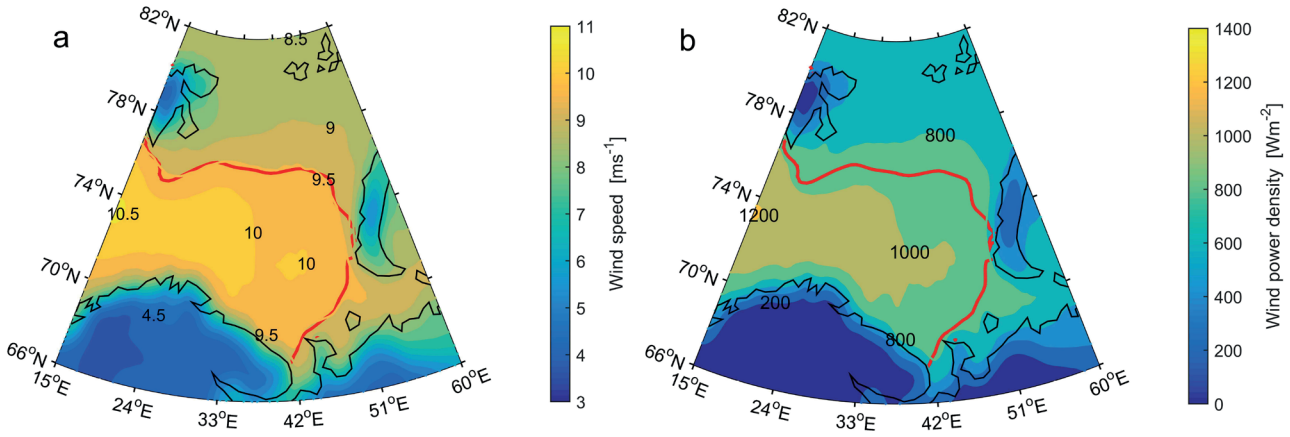

Figure 6

Spatial distributions of annual average wind speed and power density at 100 m

the largest wind power potential of more than 1600 W m^{-2} is observed in winter. It declines in summer to the lowest value of less than 400 W m^{-2}. As for the ice-free zone, the wind power density is primarily between 1200 and 1800 W m^{-2} in winter, between 800 and 1200 W m^{-2} in spring, between 1000 and 1200 W m^{-2} in autumn, and between 400 and 500 W m^{-2} in summer.

Interannual variations of wind power density

It is also meaningful to better understand the interannual variations of wind power density. Temporal variations of the annual average wind power density at the seven locations from 1996 to 2015 are shown in Figure 9 and the mean wind speed and power density at each point are shown in Table 3.

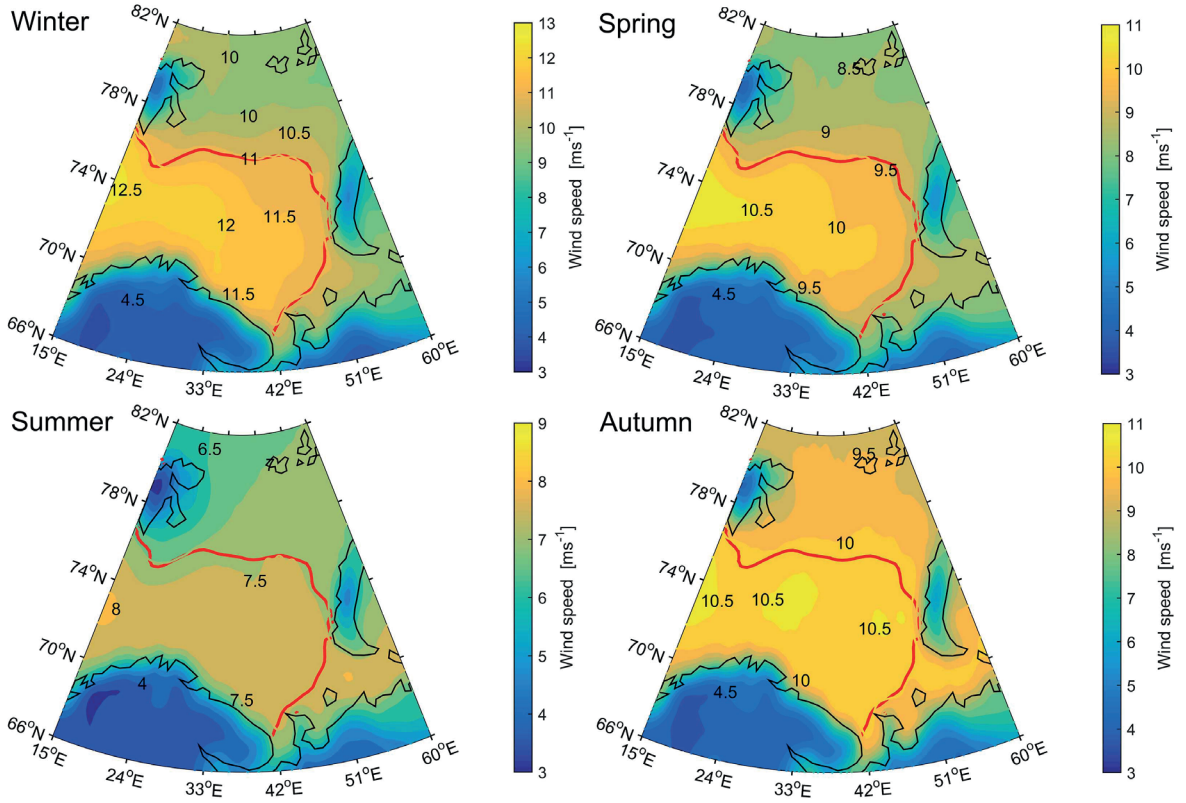

Figure 7

Spatial distributions of mean seasonal wind speed at 100 m from winter to autumn

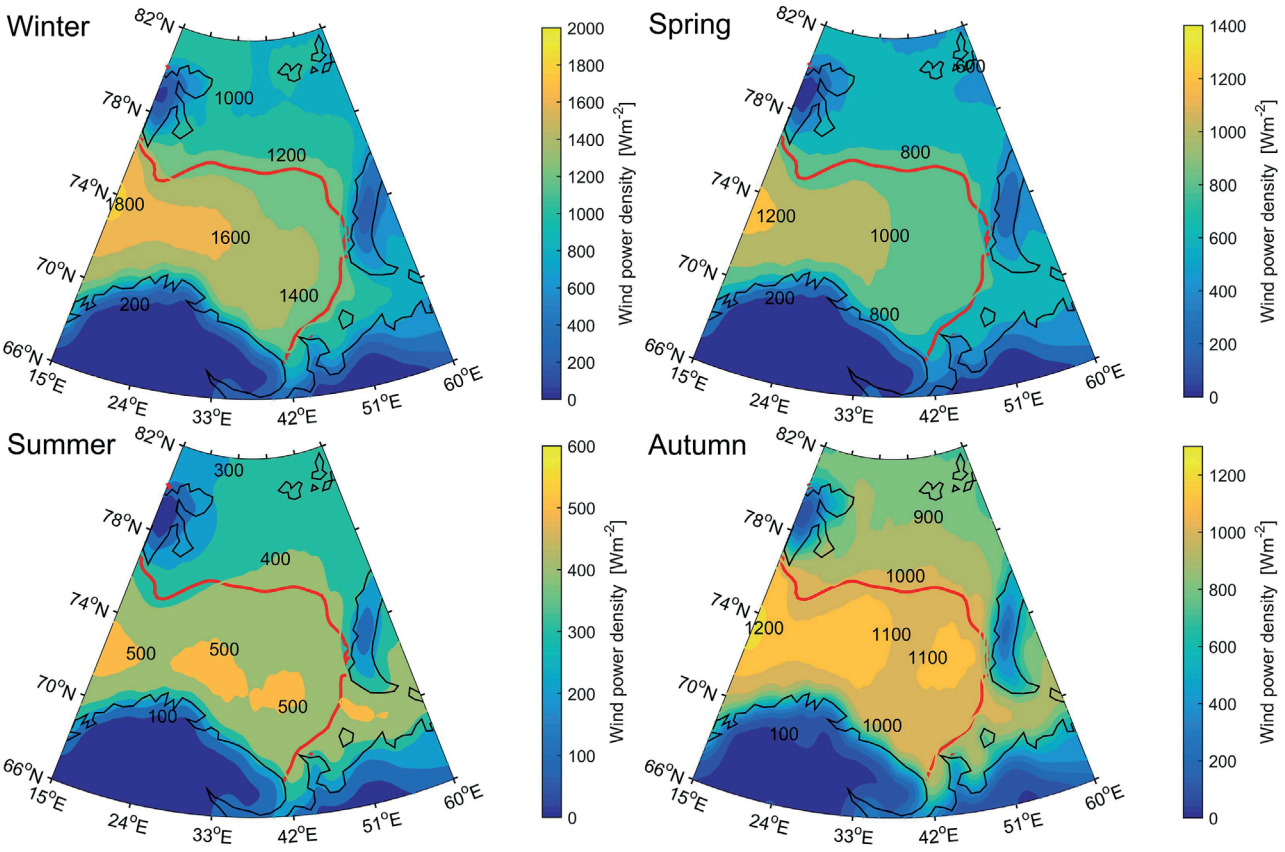

Figure 8

Spatial distributions of mean seasonal wind power density at 100 m from winter to autumn

Table 2

Parameters of model wind turbine generators for CCWE3000D and SL500

WTGs	Rated power (kW)	Hub height (m)	Rotor diameter (m)	Cut-in wind speed (m s^{-1})	Rated wind speed (m s^{-1})	Cut-out wind speed (m s^{-1})
CCWE3000D	3000	100	103	3	12	25
SL500	5000	100	128	3.5	12.5	25

Most of the selected points are with approximately 10 m s^{-1} speed and 1000 W m^{-2} power density. It appears from Figure 9 that most points show a good stability within a bias range of 200 W m^{-2}, except the occasional higher peaks in 1999, 2006, 2010 and 2015. In addition, it is also obvious that the wind is much stronger in the southwestern area characterized by the highest power potential.

Analysis of extractable gross electric energy production

In order to determine the available offshore wind energy production, two different wind turbine generators (WTGs) with rafted power 3000 and 5000 kW were chosen. The design parameters, including cut-in, rated and cut-out speeds, and two relevant power output curves are shown in Table 2 and Figure 10, respectively. Based on equation (8), the annual average net electric energy production using the two WTGs was calculated. As shown in Table 3, all selected locations in the ice-free zone can generate approximately 14 000 MWh of electricity per year using the CCWE3000D turbine and 23000 MWh using the SL500 turbine.

Discussion

Comparison with other studies and other regions

Compared to previous similar assessments, this study presents for the first time a detailed

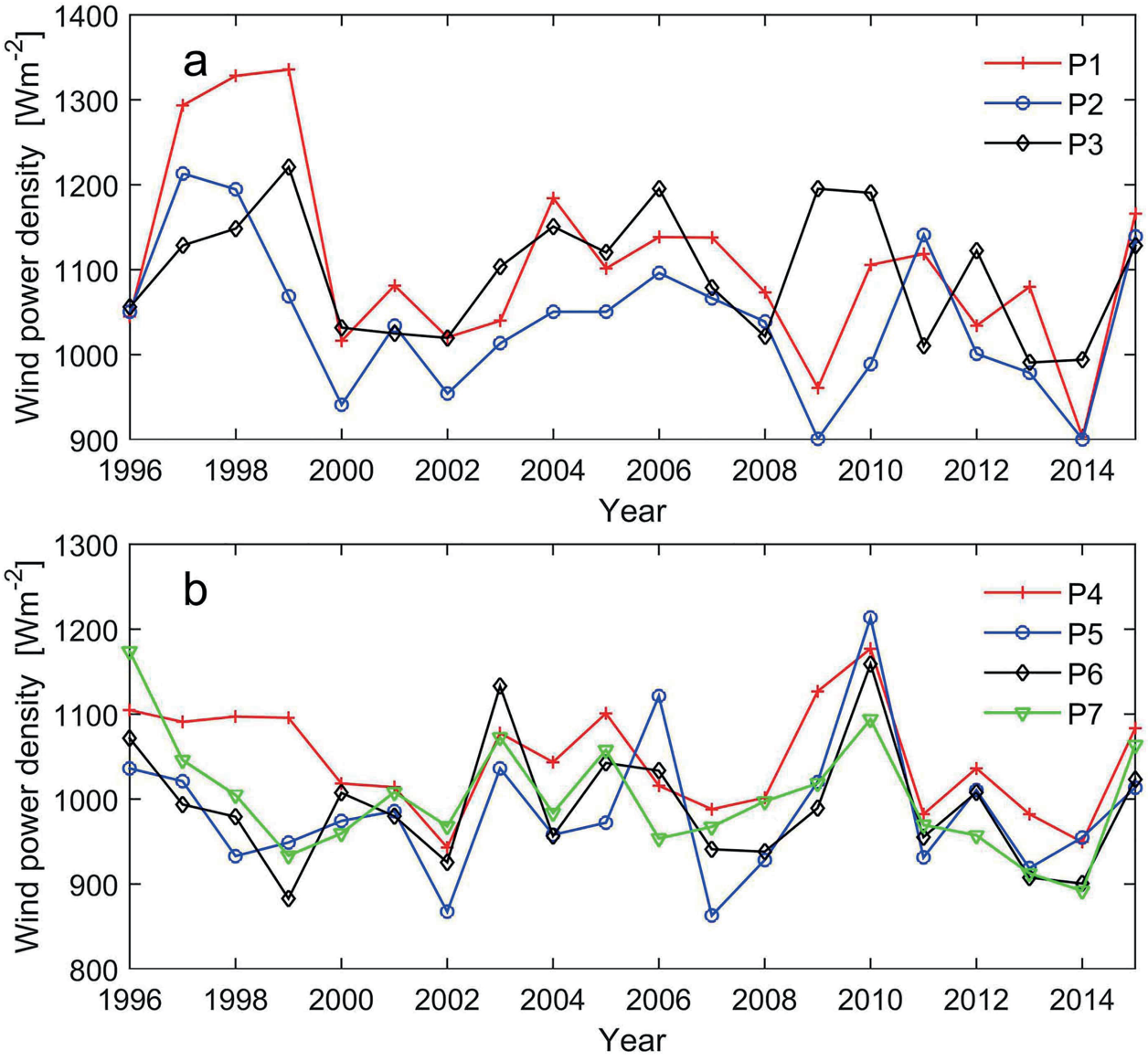

Figure 9

Interannual variations of annual average wind power density at 100 m from P1 to P7 in 1996–2015

Table 3

Locations of the selected points and 100 m annual average wind speeds, wind power density (WPD) and net electric energy output from P1 to P7

Points	Longitude (N)	Latitude (E)	Mean speed (m s^{-1})	WPD (W m^{-2})	Electric energy (MWhy)	
					CCWE3000D	SL500
P1	22	74	10.23	1108	14 384	23 534
P2	22	72	9.99	1041	14 002	22 855
P3	32	74	10.26	1097	14 535	23 776
P4	35	72	10.10	1046	14 312	23 390
P5	42	73	9.91	985	14 011	22 873
P6	42	71	9.95	991	14 121	23 064
P7	37	70	9.96	1002	14 118	23 079

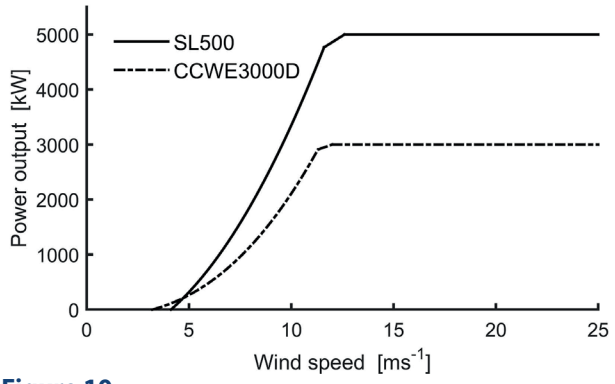

Figure 10

Power output curves for wind turbine generators

analysis and quantification of wind behavior and power potential in the Barents Sea. Liu et al. (2008) assessed the global ocean wind power at 10 m, which underestimated the power contained at the hub height. Capps & Zender (2009, 2010) firstly estimated the global usable wind power using turbines, but they did not cover zones with latitudes above 70°N. Zheng & Pan (2014) presented a grade classification of the global ocean 10 m wind power density in terms of the annual average speed based on CCMP (cross-calibrated, multi-platform) wind field data. According to the classification, the top class has an average annual speed between 7.0 and 9.4 m s^{-1}, therefore the ice-free zone of the Barents Sea is one of the zones characterized by the highest wind power density. In the ice zone, the Barents Sea has the second class assigned based on the speed standard between 6.4 and 7.0 m s^{-1}.

It should also be noted that there are some differences in wind behavior between the Barents Sea and other regions. Based on the results of wind roses, no steady wind direction frequency exceeds 10%, which means that the wind blows from every direction with no predominant direction. This wind regime is different from other low-latitude seas characterized by predominant directions, such as NW–NNW in the Ionian Sea (Karamanis et al. 2011) and ENE in the Caribbean Sea (Chadee & Clarke 2014).

Analysis of wind extreme speed parameters

Previous studies assessing the wind potential in different regions did not refer to the estimation of extreme wind speeds. However, the extreme wind conditions are likely to pose serious threats to marine structures (Holmes 2015). In other words, offshore turbines should survive the extreme speeds at long return periods, such as 50 and 100 years. Therefore, the popular GEV, Gumbel, Weibull and P-III distributions were used to fit a series of the annual maximum 10 m wind speeds at each grid point in the domain. In addition, the K-S test and RMSE were used to analyze and compare the applicability of different distributions. The results of detailed comparisons between the four distributions are presented in Table 4. The P-III distribution has the best fitness on most grids in the domain with the K-S passing rate of 100% and the minimum RMSEs. Gumbel and GEV distributions rank second, while the Weibull distribution produces the worst results.

Table 4

Comparisons of the K-S test and RMSE between GEV, Gumbel, Weibull and P-III distributions

Distributions	K-S test	Mean RMSE	Maximum RMSE	Minimum RMSE
GEV	99.97%	0.0484	0.1700	0.0210
Gumbel	99.96%	0.0591	0.1353	0.0174
Weibull	98.56%	0.0473	0.2957	0.0191
P-III	100%*	0.0434*	0.1061*	0.0153*

Note: Results of the K-S test in this study mean in fact the passing rate of all grids in the whole domain with the significance level of 0.05. The most optimal results are marked with *.

Furthermore, the fitting probability density curves and cumulative probability density curves from P1 to P7 were calculated using the four distribution functions (Fig. 11a and b). The extreme wind speeds with different return values based on P-III and Gumbel distributions from P1 to P7 are presented in Table 5. Although the P-III distribution has the best fitting effect in most grids in the domain, the Gumbel distribution shows higher extreme speeds at longer returns (Figure 11 and Table 5). This information may be useful for designers to strengthen the turbine resistance to stronger wind loads.

Moreover, spatial distributions of extreme wind speeds at 50-year and 100-year return periods based on the P-III distribution function were calculated (Fig. 12). For the 50-year return period, the wind speeds are primarily between 22 and 26 m s^{-1} in the ice-free zone and between 26 and 30 m s^{-1} in the ice zone. With regard to the 100-year return period, speeds are mainly between 22 and 28 m s^{-1} in the ice-free zone and between 28 and 32 m s^{-1} in the ice zone. It should be noted that extreme wind speeds at the 50-year and 100-year return periods in the ice-free zone are lower than those in the ice zone. Surprisingly, however, the annual average speeds in the ice-free zone are higher than those in the ice zone (see Fig. 3). This probably indicates that there are occasional stronger wind speeds in the ice zone. The contrasting phenomenon deserves further research to explain aerodynamics in depth.

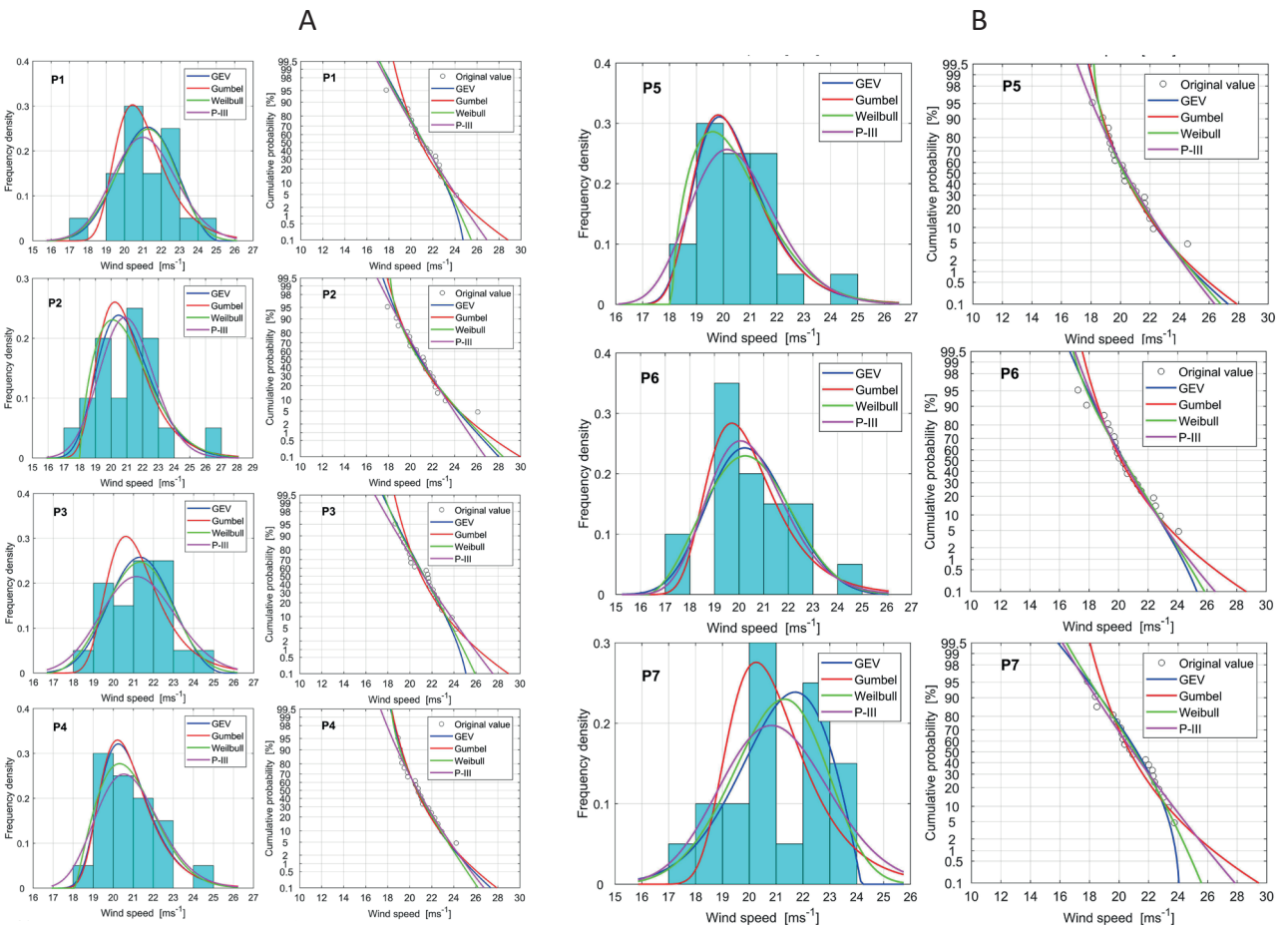

Figure 11

A. Fitting probability density curves and cumulative probability density curves of the annual maximum wind speed series from P1 to P4; B. Fitting probability density curves and cumulative probability density curves of the annual maximum wind speed series from P5 to P7

Table 5

Different return values of extreme wind speeds (m s^{-1}) based on Gumbel and P-III distributions from P1 to P7 for 50-year and 100-year return periods; higher extreme speeds are marked with *

Points	Distribution	5-year	10-year	25-year	50-year	100-year
P1	Gumbel	22.62	23.17	24.32	25.18*	26.03*
	P-III	22.59	23.39	24.27	24.85	25.38
P2	Gumbel	22.35	23.41	24.75	25.74*	26.73*
	P-III	22.47	23.27	24.15	24.73	25.26
P3	Gumbel	22.43	23.33	24.48	25.33*	26.17*
	P-III	22.86	23.73	24.68	25.30	25.88
P4	Gumbel	21.89	22.73	23.78	24.57*	25.34*
	P-III	22.16	22.97	23.87	24.49	25.06
P5	Gumbel	21.57	22.45	23.56	24.38*	25.20*
	P-III	21.78	22.58	23.49	24.11	24.68
P6	Gumbel	21.65	22.62	23.85	24.76*	25.67*
	P-III	21.76	22.58	23.52	24.16	24.76
P7	Gumbel	22.26	23.26	24.52	25.46*	26.39*
	P-III	22.71	23.66	24.71	25.40	26.03

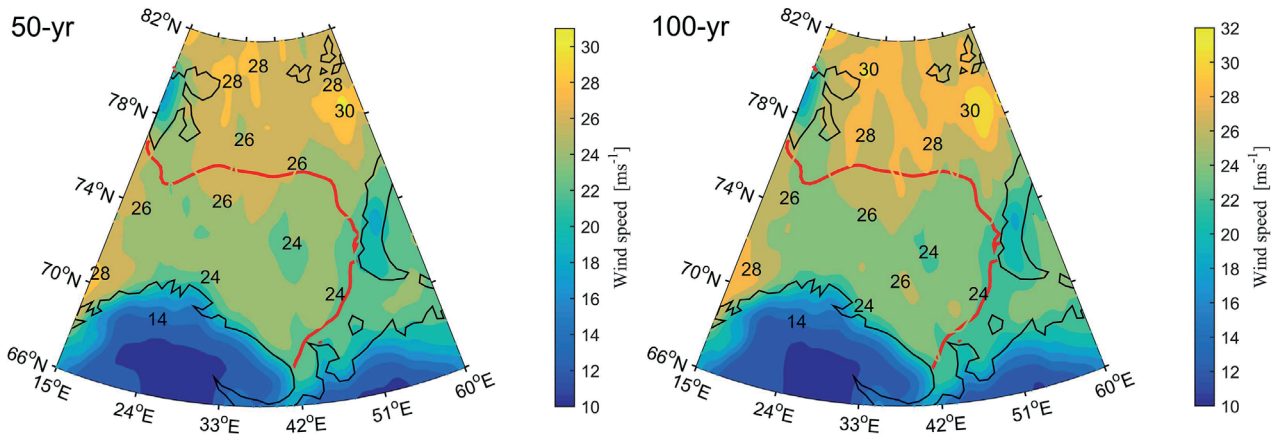

Figure 12

Spatial distributions of extreme wind speeds in 50-year and 100-year return periods based on the P-III distribution function

Conclusions

The Barents Sea has been divided into the ice-free zone and the ice zone based on the NSIDC monthly sea ice cover. The ice-free zone preserves open-water conditions throughout the year and there are hardly any serious threats caused by drift or floating ice.

The wind speeds at 10 m decrease from southwest to northeast in the Barents Sea. The wind offshore is generally stronger than near the shore. The highest mean monthly wind speeds are in winter and the lowest in summer, with a high seasonal variation. Moreover, the wind directional distributions are relatively equal and no steady wind direction can be regarded as a prevailing direction. Furthermore, the available wind power potential at a hub height of 100 m was calculated. The 100 m wind speeds and wind power density show similar spatio-temporal variation as the 10 m wind. The annual average wind speeds between 8.5 and 10.5 m s^{-1} with power density between 600 and 1200 W m^{-2} occur in most parts of the entire domain. At most selected points, the average wind power density shows a good stability within a bias range of 200 W m^{-2}. All the selected locations in the ice-free zone can generate approximately 14 000 MWh of electricity per year based on the 3000 kW turbine and 23 000 MWh based on the 5000 kW turbine. Moreover, the Pearson type III distribution has the best fitting effect in the annual maximum wind speed series in the domain and the Gumbel distribution gives higher extreme values at longer return periods.

In summary, this paper promotes the understanding of wind conditions in the Barents Sea and presents a statistical assessment of wind energy resources using the ECMWF ERA-Interim datasets from 1996 to 2015. Further research may be needed in the future to reduce the uncertainty using more data derived from measurements and observations.

Acknowledgements

The authors are grateful to the reviewers for their valuable comments and suggestions that have helped to improve the paper. The work is financially supported by the National Natural Science Foundation of China (No. 51779236 and 51509226) and the National Key R&D Program of China (No. 2016YFC0303401).

References

Alimi, S.E., Maatallah, T., Dahmouni, A.W. & Nasrallah, S.B. (2012). Modeling and investigation of the wind resource in the gulf of Tunis, Tunisia. *Renewable & Sustainable Energy Reviews* 16(8): 5466–5478.

Ban, M., Perković, L., Duić, N. & Penedo, R. (2013). Estimating the spatial distribution of high altitude wind energy potential in Southeast Europe. *Energy* 57(3): 24–29.

Capps, S.B. & Zender, C.S. (2009). Global ocean wind power sensitivity to surface layer stability. *Geophysical Research Letters* 36(9). DOI: 10.1029/2008GL037063.

Capps, S.B. & Zender, C.S. (2010). Estimated global ocean wind power potential from QuikSCAT observations, accounting for turbine characteristics and siting. *Journal of Geophysical Research: Atmospheres* 115(D9). DOI: 10.1029/2009JD012679.

Chadee, X.T. & Clarke, R.M. (2014). Large-scale wind energy potential of the Caribbean region using near-surface reanalysis data. *Renewable and Sustainable Energy Reviews* 30: 45–58.

Dee, D.P., Uppala, S.M., Simmons, A.J., Berrisford, P., Poli, P. et al. (2011). The ERA-Interim reanalysis: Configuration and performance of the data assimilation system. *Quarterly Journal of the royal meteorological society* 137(656): 553–597.

Dee, D.P. & Uppala, S. (2009). Variational bias correction of satellite radiance data in the ERA-Interim reanalysis. *Quarterly Journal of the Royal Meteorological Society* 135(644): 1830–1841.

Divine, D.V. & Dick, C. (2006). Historical variability of sea ice edge position in the Nordic Seas. *Journal of Geophysical Research: Oceans* 111(C1). DOI: 10.1029/2004JC002851.

Eriksson, S., Bernhoff, H. & Leijon, M. (2008). Evaluation of different turbine concepts for wind power. *Renewable & Sustainable Energy Reviews* 12(5): 1419–1434.

Eurek, K., Sullivan, P., Gleason, M., Hettinger, D., Heimiller, D. et al. (2017). An improved global wind resource estimate for integrated assessment models. *Energy Economics* 64: 552–567.

Fyrippis, I., Axaopoulos, P.J. & Panayiotou, G. (2010). Wind energy potential assessment in Naxos Island, Greece. *Applied Energy* 87(2): 577–586.

Gasparatos, A., Doll, C.N., Esteban, M., Ahmed, A. & Olang, T.A. (2017). Renewable energy and biodiversity: Implications for transitioning to a Green Economy. *Renewable & Sustainable Energy Reviews* 70: 161–184.

Herbaut, C., Houssais, M.N., Close, S. & Blaizot, A.C. (2015). Two wind-driven modes of winter sea ice variability in the Barents Sea. *Deep Sea Research Part I: Oceanographic Research Papers* 106: 97–115.

Holmes, J.D. (2015). *Wind loading of structures*. CRC press. pp: 49–53.

Hodges, K.I., Lee, R.W. & Bengtsson, L. (2011). A comparison of extratropical cyclones in recent reanalyses ERA-Interim, NASA MERRA, NCEP CFSR, and JRA-25. *Journal of Climate* 24(18): 4888–4906.

Hsu, S.A., Meindl, E.A. & Gilhousen, D.B. (1994). Determining the power-law wind-profile exponent under near-neutral stability conditions at sea. *Journal of Applied Meteorology* 33(6): 757–765.

Ingvaldsen, R.B., Asplin, L. & Loeng, H. (2004). Velocity field of the western entrance to the Barents Sea. *Journal of Geophysical Research: Oceans* 109(C3). DOI: 10.1029/2003JC001811.

Karamanis, D., Tsabaris, C., Stamoulis, K. & Georgopoulos, D. (2011). Wind energy resources in the Ionian Sea. *Renewable Energy* 36(2): 815–822.

Kwok, R. (2009). Outflow of Arctic Ocean sea ice into the Greenland and Barents Seas: 1979–2007. *Journal of Climate* 22(9): 2438–2457.

Lien, V.S., Schlichtholz, P., Skagseth, Ø. & Vikebø, F.B. (2017). Wind-Driven Atlantic Water Flow as a Direct Mode for Reduced Barents Sea Ice Cover. *Journal of Climate* 30(2): 803–812.

Liu, W.T., Tang, W. & Xie, X. (2008). Wind power distribution over the ocean. *Geophysical Research Letters* 35(13). DOI: 10.1029/2008GL034172.

Onea, F., Raileanu, A. & Rusu, E. (2015). Evaluation of the wind energy potential in the coastal environment of two enclosed seas. *Advances in Meteorology.* 2015. DOI: 10.1155/2015/808617.

Panofsky, H.A. & Dutton, J.A. (1984). *Atmospheric Turbulence*. Wiley, 397 pp.

Pavlova, O., Pavlov, V. & Gerland, S. (2014). The impact of winds and sea surface temperatures on the Barents Sea ice extent, a statistical approach. *Journal of Marine Systems* 130: 248–255.

Perković, L., Silva, P., Ban, M., Kranjčević, N. & Duić, N. (2013). Harvesting high altitude wind energy for power production: The concept based on Magnus' effect. *Applied energy* 101: 151–160.

Reistad, M., Breivik, Ø., Haakenstad, H., Aarnes, O.J., Furevik, B.R. et al. (2011). A high-resolution hindcast of wind and waves for the North Sea, the Norwegian Sea, and the Barents Sea. *Journal of Geophysical Research: Oceans* 116(C5). DOI: 10.1029/2010JC006402.

Shapiro, I., Colony, R. & Vinje, T. (2003). April sea ice extent in the Barents Sea, 1850–2001. *Polar Research* 22(1): 5–10.

Simionato, C.G., Vera, C.S. & Siegismund, F. (2005). Surface wind variability on seasonal and interannual scales over Río de la Plata area. *Journal of Coastal Research* 21(4): 770–783.

Szczypta, C., Calvet, J.C., Albergel, C., Balsamo, G., Boussetta, S. et al. (2011). Verification of the new ECMWF ERA-Interim reanalysis over France. *Hydrology and Earth System Sciences* 15(2): 647.

Wang, Z., Dong, S., Dong, X. & Zhang, X. (2016). Assessment of wind energy and wave energy resources in Weifang sea area. *International Journal of Hydrogen Energy* 41(35): 15805–15811.

Yang, W., Tavner, P.J., Crabtree, C.J., Feng, Y. & Qiu, Y. (2014). Wind turbine condition monitoring: technical and commercial challenges. *Wind Energy* 17(5): 673–693.

Zheng, C.W. & Pan, J. (2014). Assessment of the global ocean wind energy resource. *Renewable and Sustainable Energy Reviews* 33: 382–391.

Zheng, C.W., Pan, J. & Li, J.X. (2013). Assessing the China Sea wind energy and wave energy resources from 1988 to 2009. *Ocean Engineering* 65: 39–48.